Modified continuum model for stability analysis of asymmetric FGM double-sided NEMS: Corrections due to finite conductivity…

Article *in* Composites Part B Engineering · July 2015

DOI: 10.1016/j.compositesb.2015.08.029

CITATIONS
21

READS
217

3 authors, including:

Hamid M Sedighi
Shahid Chamran University of Ahvaz
77 PUBLICATIONS **590** CITATIONS
SEE PROFILE

Mohamadreza Abadyan
Shahrekord Branch, Islamic Azad University
93 PUBLICATIONS **1,151** CITATIONS
SEE PROFILE

Composites Part B 83 (2015) 117–133

Contents lists available at ScienceDirect

Composites Part B

journal homepage: www.elsevier.com/locate/compositesb

Modified continuum model for stability analysis of asymmetric FGM double-sided NEMS: Corrections due to finite conductivity, surface energy and nonlocal effect

Hamid M. Sedighi [a], Maryam Keivani [b], Mohamadreza Abadyan [c, *]

[a] Mechanical Engineering Department, Faculty of Engineering, Shahid Chamran University of Ahvaz, Iran
[b] Shahrekord University of Medical Sciences, Shahrekord, Iran
[c] Shahrekord Branch, Islamic Azad University, Shahrekord, Iran

ARTICLE INFO

Article history:
Received 5 March 2015
Received in revised form
8 May 2015
Accepted 6 August 2015
Available online 20 August 2015

Keywords:
C. Micro-mechanics
A. Nano-structures
B. Vibration

ABSTRACT

Finite conductivity, surface energy and nonlocal effect can influence the electromechanical performance of micro/nano-electromechanical systems (MEMS/NEMS). However, these factors are yet ignored on stability analysis of MEMS/NEMS fabricated from functionally graded materials (FGM). In this paper, dynamic stability of double-sided NEMS fabricated from non-symmetric FGM is investigated incorporating finite conductivity, surface energy and nonlocal effect. The Gurtin–Murdoch model and Eringen's elasticity are employed to consider the surface energy and nonlocal effect, respectively. Effect of finite conductivity of FGM on electrostatic and Casimir attractions is incorporated via relative permittivity and plasma frequency of the material. The stability analysis of the nanostructure is conducted by plotting time history and phase portraits. Moreover, bifurcation analysis is conducted to investigate the stability of the fixed points of the nano-structure. The validity of the proposed model is examined by comparing the results of the present study with those reported in the literature. The impact of various parameters i.e. finite conductivity, nonlocal parameter, surface stresses and material characteristics on the dynamic instability of the NEMS are addressed.

1. Introduction

With recent developments in nano-scale manufacturing technologies, functionally graded materials (FGMs) are being considered as potential structural materials with promising applications in optoelectronics, biomechanics, tribology and micro/nanotechnology [1,2]. Functionally Graded Materials belong to a class of advanced materials with continuously varying properties over the thickness. The graded properties of FGMs result in high resistance to temperature gradients and significant reduction in the stress concentrations, thermal stresses and residual stresses. Due to the inherent properties of FGMs as the multi-functional materials, these advanced composites are very good candidates for smart structures. Interestingly, FGMs have received considerable attention in developing ultra-small systems and miniature devices. Previous researchers have theoretically addressed the mechanical behavior of FGM miniature elements. Eltaher et al. [3] studied the static bending and buckling of functionally graded nanobeams. They indicated that, the material-distribution profile may be manipulated to change the maximum deflection and maximize the critical buckling load. Ke and Wang [4] investigated dynamic stability of FGM micro-beams using the modified couple stress theory. Nonlinear finite element model of functionally graded micro-beams by considering the power-law variation of material through the beam height, and microstructure length scale parameter was developed by Arbind and Reddy [5] for the Euler–Bernoulli and the Timoshenko beam theories. They demonstrated that the effect of micro-structural parameter is to stiffen the micro-beams. The vibration of axially functionally graded material (AFGM) nanobeam was investigated by Zeighampour and Tadi Beni [6] by employing strain gradient theory. They studied the impacts of the diameter of the nanobeam, the stiffness and damping of the visco-Pasternak foundation on the natural frequency of the nanobeams. With recent growth in micro/nano-fabrication technology, FGMs are explored for constructing micro/

* Corresponding author.
E-mail addresses: hmsedighi@gmail.com, h.msedighi@scu.ac.ir (H.M. Sedighi), Maryam.Keivani@yahoo.com (M. Keivani), abadyan@yahoo.com (M. Abadyan).

http://dx.doi.org/10.1016/j.compositesb.2015.08.029
1359-8368/

nano-electromechanical systems (MEMS/NEMS) [7–9]. In this regard, some researchers have focused on modeling FGM-fabricated MEMS/NEMS. Abbasnejad et al. [10] studied the mechanical behavior of a fixed–fixed FGM micro-beam subjected to a nonlinear electrostatic pressure using modified couple stress theory and classic theory. They showed that by increasing the power law constant, the position of the saddle node bifurcation moves to the right in the state-space. Ji et al. [11] investigated the pull-in instability and free vibration of functionally graded poly-SiGe microbeams under combined electrostatic force and axial residual stress, with an emphasis on the effects of ground electrode shape. The dynamic pull-in behavior of FGM nano-actuators has been previously addressed by the authors [12] using classical continuum elasticity. In present article, a modified continuum model is proposed to investigate the pull-in instability of double-sided beam-type NEMS bridges made of asymmetric FGM beam. Three important modifications are considered in order to increase the accuracy of the model.

The first modification is incorporating the finite conductivity of FGMs in the equation of motion of the nano-bridge. It is well established that for precise simulation of NEMS, both Casimir and Coulomb forces should be considered in deriving the governing equation [13]. The strength of Casimir and Coulomb forces between interacting surfaces strongly depends on the material characteristics of the surfaces [14,15]. Correction of Casimir force due to finite conductivity of the interacting flat plates have been calculated to first order by Hargraves [16] and to second order by Bezerra et al. [17]. These researchers have proposed simple approximations for Casimir force as a function of plasma wavelength of material. Similar to Casimir force, the Coulomb attraction between two FGM plates (with finite conductivity) is less than that of perfect metals. The corrected Coulomb force for FGM NEMS can be obtained considering the dielectric characteristics (permittivity) of FGM. It should be mentioned that all the previous researchers who investigated FGM NEMS have used force relations that are valid only for perfectly conductive metals. However, this is not acceptable for graded materials especially ceramic-metal FGMs. Herein, the finite conductivity of FGM is taken into account for computing Coulomb attraction between surfaces as well as Casimir force.

The second correction is due to the presence of surface layer that affects the elastic stiffness of the micro-/nano-beams. The experimental results have demonstrated that for nanoscale structures, the surface effects become significant due to the high surface/volume ratio [18]. Gurtin and Murdoch [19] developed a surface elasticity theory for isotropic materials that model the surface layer of a solid as a membrane with negligible thickness. A size-dependent finite element model, for Mindlin plate theory accounting for the position of the neutral plane for continuum incorporating surface energy effect, was proposed by Shaat et al. [20] to study the bending behavior of ultra-thin FGM plates. Wang et al. [21] summarized the advances in the surface stress effect in mechanics of nano-structured elements, including nanowires, nanobeams, and nano-films. Sedighi [22] investigated the dynamic pull-in instability of nonlocal nano-bridges incorporating the surface effect and intermolecular forces. The influence of surface effects on the pull-in instability of a cantilever nano-actuators was investigated by Koochi et al. [23] incorporating the effect of Casimir attraction. Ansari et al. [24] examined the instability characteristics of hydrostatically and electrostatically actuated circular nanoplates including surface stress effect on the basis of Gurtin–Murdoch elasticity theory. Hosseini-Hashemi and Nazemnezhad [25] studied the nonlinear free vibration of simply supported FG nanoscale beams with considering surface effects. They discussed the influences of the FG nanobeam length, volume fraction index, amplitude ratio, mode number and thickness ratio on the normalized nonlinear natural frequencies of the FG nanobeams. In the current study, the impact of surface layer on the pull-in behavior of FGM nano-bridges is taken into account.

The third modification that is considered in the proposed model is the nonlocal effects that appears at micro/nanoscales. In order to modeling the nonlocal effects, size-dependent continuum theory such as Eringen elasticity has been proposed for modeling the size phenomenon in nanostructures [26]. This theory has been employed to investigate the size dependent behavior of miniature structures. Li et al. [27] presented the analytical solution for the transverse vibration of nano-beams subjected to initial axial force based on the nonlocal theory. To simulate transient thermo-elastic responses of the nanostructure subjected to a sudden thermal loading, Yu et al. [28] extended the classical thermo-elastic models using Eringen's nonlocal elasticity and Caputo fractional derivative and memory dependent derivative (MDD). Reddy and El-Borgi [29] derived the governing equations of Timoshenko beams assuming the Eringen's nonlocal differential model and modified von Kármán nonlinear strains. They also developed the finite element models of the resulting equations and presented the numerical results for various boundary conditions, showing the effect of the nonlocal parameter on the deflections. Kiani [30] studied the axial buckling behavior of vertically aligned single-walled carbon nanotubes based on the nonlocal continuum theory and addressed the roles of the influential factors on both in-plane and out-of-plane axial buckling loads. Jung et al. [31] employed the modified couple stress theory which accounts for the asymmetric couple stress tensor, for buckling analysis of S-FGM nanoplates embedded in Pasternak elastic medium. They addressed the effects of power law index, small scale coefficient, aspect ratio, side-to-thickness ratio, loading types, and elastic medium parameter on the buckling load of S-FGM nanoplates. Ebrahimi and Salari [32] employed the nonlocal Euler–Bernoulli beam theory for vibration analysis of functionally graded (FG) size-dependent nanobeams by using Navier-based analytical method and investigated the effects of systems parameters on the normalized natural frequencies of the FG nanobeams. In another research [33] they studied the thermal effect on free vibration characteristics of functionally graded (FG) size-dependent nanobeams subjected to an in-plane thermal loading using the same method of solution. The nonlocal elasticity has also been applied for simulating the pull-in instability of MESM/NEMS actuators fabricated from isotropic material. In this research work, the Eringen elasticity is employed for considering the influence of nonlocal effects on the pull-in characteristics of the double-sided nano-bridge.

The present article is organized to study the effects of finite conductivity of FGMs on the dynamic instability of double-sided NEMS bridge considering the surface energy and nonlocal effects. To this end, the influences of actuation voltages, nonlocal parameter, properties of FGM materials, surface stresses and Casimir force on the pull-in parameters are investigated. To verify the soundness of the present analysis, the obtained results are compared with the reported results in the literature.

2. Mathematical modeling

Fig. 1 depicts an asymmetric functionally graded nano-bridge actuated by a pair of parallel-plate electrodes with length l, thickness h, width b and initial gaps g_1 and g_2 from the bottom and top substrates which is under DC actuation voltages V_1 and V_2, respectively. The distance of any point of the nano-beam from the neutral axis and the top surface are represented by z and $\tilde{z}$, respectively. Moreover, the distance of the neutral axis from the top surface is denoted by $\tilde{z}_c$. The coordinate system is also illustrated in Fig. 1.

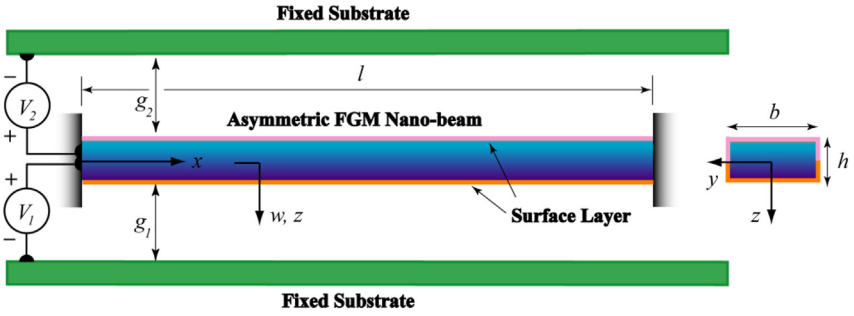

Fig. 1. Configuration of a non-classical asymmetric FGM nano-bridge.

It is assumed that the lower surface of the FGM nano-beam is made of perfectly conductive material (such as metal) and the upper surface is made of finite conductive material (such as dielectric). The typical material property P of nano-structure is varied through the beam thickness according to the volume fraction rule described as follows:

$$P(z) = P^{+}V^{+}(z) + P^{-}V^{-}(z) \tag{1}$$

in which superscripts $-$ and $+$ refer to the perfectly conductive and finite conductive constituents, respectively, V is the volume fraction and $P(z)$ is an arbitrary material property of the nano-structure. Therefore, based on the power law distribution, the material properties can be expressed by the following formula [34]:

$$E(\tilde{z}) = E^{+} + \left(\frac{\tilde{z}}{h}\right)^{n}\left(E^{-} - E^{+}\right) \tag{2-a}$$

$$\rho(\tilde{z}) = \rho^{+} + \left(\frac{\tilde{z}}{h}\right)^{n}\left(\rho^{-} - \rho^{+}\right) \tag{2-b}$$

$$\chi(\tilde{z}) = \chi^{+} + \left(\frac{\tilde{z}}{h}\right)^{n}\left(\chi^{-} - \chi^{+}\right) \tag{2-c}$$

where E is the modulus of elasticity, ρ is the density of nano-beam and $\chi = 1/\varepsilon$, in which the parameter ε is the relative permittivity of dielectric (finite conductive) medium and the gradient index n determines the type of the variation of the properties along the thickness. Fig. 2 details the variation of V^{+} (volume fraction of finite conductive constituent) through-the-thickness for different values of gradient power n.

2.1. Surface stresses

To model the surface energy, the nano-bridge is divided into three laminated layers, including two surface layers and a core (bulk) layer. The modulus of elasticity for the surface layer is represented by E_0 which can be determined from atomistic calculations. It is assumed that there is no residual stress in the bulk FGM due to surface tension; so the corresponding bulk stress–strain relations of the beam can be expressed as:

$$\sigma_{xx} = E(\tilde{z})\varepsilon_{xx} + \nu\sigma_{zz} \tag{3}$$

where ν is the Poisson's ratio of nano-beam. In classical theory, the stress component σ_{zz} is assumed to be equal to zero. However, when the surface stress is taken in to consideration, the equilibrium relation will not be satisfied with this assumption. In this case, the stress component σ_{zz} is expressed as follows [35]:

$$\sigma_{zz} = \frac{1}{2}\left(\sigma_{zz}^{+} + \sigma_{zz}^{-}\right) + \frac{z}{h}\left(\sigma_{zz}^{+} - \sigma_{zz}^{-}\right) \tag{4}$$

where σ_{zz}^{+} and σ_{zz}^{-} are stresses at the top and bottom surface layers, respectively. The stresses of the surface layer satisfy the following equilibrium relation [36]:

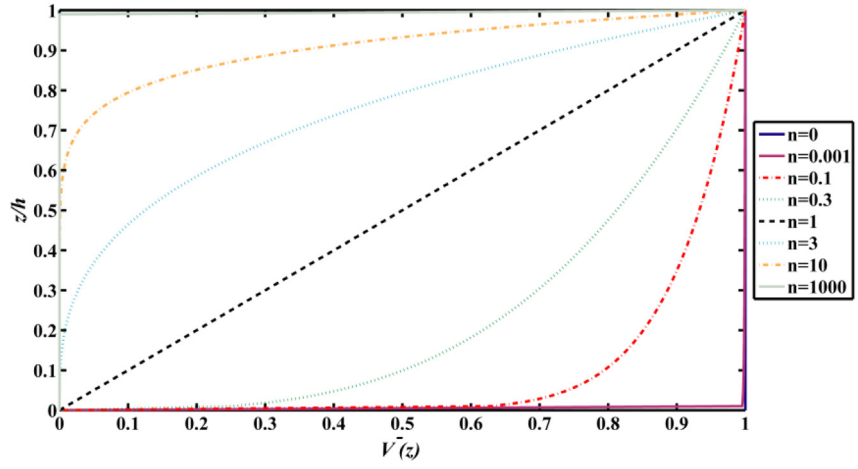

Fig. 2. Distribution of the volume fraction of finite conductive constituent (V^{+}) through the thickness for different gradient index n values.

$$\sigma_{zz} = \frac{1}{2}\left[\left(\tau_0^+ - \tau_0^-\right)\left(\frac{\partial^2 w}{\partial x^2}\right) - \left(\rho_0^+ - \rho_0^-\right)\left(\frac{\partial^2 w}{\partial t^2}\right)\right] + \frac{z}{h}\left[\left(\tau_0^+ + \tau_0^-\right)\left(\frac{\partial^2 w}{\partial x^2}\right) - \left(\rho_0^+ + \rho_0^-\right)\left(\frac{\partial^2 w}{\partial t^2}\right)\right] \tag{5}$$

Moreover, the constitutive equations for the surface layers developed by Gurtin and Murdoch [19] are written as:

$$\tau_{xx} = \tau_0 + E_0\frac{\partial u}{\partial x},\ \tau_{zx} = \tau_0\frac{\partial w}{\partial x} \tag{6}$$

where τ_{xx} and τ_{zx} are non-zero membrane stresses exist on the contact surfaces between the FG bulk material and surface layers. The stresses of the surface layers must satisfy the following equilibrium relations:

$$\left(\frac{\partial \tau_{\beta i}}{\partial \beta}\right)^+ = \sigma_{iz}^+ + \rho_0^+\left(\frac{\partial^2 u_i}{\partial t^2}\right)^+ \tag{7-a}$$

$$\left(\frac{\partial \tau_{\beta i}}{\partial \beta}\right)^- = \sigma_{iz}^- + \rho_0^-\left(\frac{\partial^2 u_i}{\partial t^2}\right)^- \tag{7-b}$$

where $\beta = x, y$ and $i = x, y, z$, $u_i^+ = u_i(z = h/2)$ and $u_i^- = u_i(z = -h/2)$ denote the displacement of surface layers in the i-direction.

2.2. Eringen nonlocal elasticity

In the classical theory, the stress at a point is related to the strain at the same point while in the Eringen's non-local elasticity theory [26], the stress at a point is a function of strains at all points of the body. The relation between the non-local stress tensor and the strain tensor is written as:

$$\sigma_{ij}(\mathbf{x}) = \int_V \alpha(|\mathbf{x}' - \mathbf{x}|, \tau) C_{ijkl}(\mathbf{x}')\varepsilon_{kl}(\mathbf{x}')dV(\mathbf{x}') \tag{8-a}$$

$$\varepsilon_{ij} = \frac{1}{2}(u_{i,j} + u_{j,i}) \tag{8-b}$$

where $\alpha(|\mathbf{x}'-\mathbf{x}|, \tau)$ is the nonlocal kernel function (nonlocal modulus) which gives the long range interactions specifying the nonlocal effects at a reference point $\mathbf{x}$ produced by the local strain at the source $\mathbf{x}'$ [37], $|\mathbf{x}'-\mathbf{x}|$ is the Euclidean distance, $C_{ijkl}(\mathbf{x})$ is the elastic modulus tensor, $\varepsilon_{ij}(\mathbf{x})$ is the strain tensor, u_i is the displacement vector, $\tau = e_0 a/l$ is the material constant where e_0 and a represent the nonlocal effects depend on the material and an internal characteristic length nanoscale. When the internal characteristic length is negligible compared to external characteristic length, τ approaches to zero and hence nonlocal elasticity theory reduces to classical elasticity theory. Eringen [26] assumed that the nonlocal modulus α can be expressed as a Green's function of a linear differential operator as follows:

$$L\alpha(|\mathbf{x}' - \mathbf{x}|, \tau) = \delta(\mathbf{x}' - \mathbf{x}) \tag{9}$$

It is demonstrated that by applying the linear operator $L = (1-\tau^2 l^2 \nabla^2)$ on the integral constitutive equation (9), it is simplified to the following partial differential equation namely the nonlocal constitutive formulation:

$$\left(1 - \tau^2 l^2 \nabla^2\right)\sigma_{ij} = C_{ijkl}\varepsilon_{kl} \tag{10}$$

where $\nabla^2 = \partial^2/\partial x^2$ is the Laplacian operator for the beam type structures. As mentioned earlier, the properties of functionally graded materials vary along the thickness of the body. Hence, for a nonlocal FG beam, Eq. (10) can be written as:

$$\sigma_{xx} - e_0^2 a^2 \frac{\partial^2 \sigma_{xx}}{\partial x^2} = \left(E^+ + \left(\frac{\tilde{z}}{h}\right)^n \left(E^- - E^+\right)\right)\varepsilon_{xx} \tag{11}$$

By assuming the identical nonlocal parameter for both FG material and surface layer, the non-local constitutive relations for the nano-scale beams can be written as follows [38]:

$$\left(1 - e_0^2 a^2 \nabla^2\right)M^{nl} = M \tag{12}$$

$$\left(1 - e_0^2 a^2 \nabla^2\right)\tau_{xx}^{nl} = \tau_{xx} \tag{13}$$

$$\left(1 - e_0^2 a^2 \nabla^2\right)\tau_{zx}^{nl} = \tau_{zx} \tag{14}$$

where the superscript "*nl*" denotes the nonlocal parameters.

2.3. Finite conductivity

The transverse load per unite length of the nanobeam $q(x,t)$ includes the electrostatic actuation $F_e(x,t)$ and Casimir attraction $F_C(x,t)$ from the lower and upper plates.

2.3.1. Coulomb force correction

The Coulomb force between parallel perfect conductive surfaces can be obtained from capacitive model. In the case of dielectric (finite conductive) interacting surfaces, the gap should be replaced with effective gap [39]. Considering the fringing field correction, the distributed electrostatic force from lower and upper plates can be expressed as:

$$F_{es,1} = \frac{b\varepsilon_0 V_1^2}{2(g_1 - w)^2}\left(1 + 0.65\frac{g_1 - w}{b}\right) \tag{15-a}$$

$$F_{e,2} = -\frac{b\varepsilon_0 V_2^2}{2(\bar{g}_2 + w)^2}\left(1 + 0.65\frac{\bar{g}_2 + w}{b}\right) \tag{15-b}$$

where $\varepsilon_0 = 8.854 \times 10^{-12}\ C^2\ N^{-1}\ m^{-2}$ represent permittivity of vacuum. In above relation, the effective gap $\bar{g}_i$ which accounts for the dielectric characteristics of FGM is written as:

$$\bar{g}_2 = g_2 + \int_0^h \chi^r dz = g_2 + \frac{h}{\varepsilon^{r+}}\left(\frac{n}{n+1}\right) \tag{16}$$

and ε^{r+} is the relative permittivity of finite conductive layer

2.3.2. Casimir force correction

As mentioned earlier, if the initial gap between the rigid plate and the electrode is on the order of several 10 nm, the Casimir forces exerted from the lower and upper substrates should be taken into account. Previous researchers analyzed the Casimir attraction between mirrors with arbitrary frequency-dependent reflectivity and found that it is always smaller than that between perfect conductive reflectors [40]. For more precise modeling of Casimir force in FGM structures one might

use the following second order corrected equations that consider the finite conductivity of the material in the theoretical model [41]:

$$F_{C,1}(x,t)=\frac{\pi^2\hbar bc}{240(g_1-w)^4} \tag{17-a}$$

$$F_{C,2}(x,t)=-\frac{\pi^2\hbar bc}{240(g_2+w)^4}\left[1-\frac{16c}{3\omega_p(g_2+w)}+\frac{24c^2}{\omega_p^2(g_2+w)^2}\right] \tag{17-b}$$

where $\hbar=1.055\times10^{-34}$ is the Planck's constant divided by 2π and $(1-e_0^2a^2\partial^2/\partial x^2)$ m/s is the speed of light [25]. In the above equation, ω_p is the plasma frequency which is proportional to the effective free-electron density in the material [42].

Thereby, the contribution of the two plates can be introduced by an effective distributed loading F_e and F_C as:

$$F_e=F_{e,1}+F_{e,2}=\frac{b\varepsilon_0V_1^2}{2(g_1-w)^2}\left(1+0.65\frac{g_1-w}{b}\right)-\frac{b\varepsilon_0V_2^2}{2(\overline{g}_2+w)^2}\left(1+0.65\frac{\overline{g}_2+w}{b}\right) \tag{18-a}$$

$$F_C=F_{C,1}+F_{C,2}=\frac{\pi^2\hbar bc}{240(g_1-w)^4}-\frac{\pi^2\hbar bc}{240(g_2+w)^4}\times\left[1-\frac{16c}{3\omega_p(g_2+w)}+\frac{24c^2}{\omega_p^2(g_2+w)^2}\right] \tag{18-b}$$

2.4. Governing equation of motion

In this section, the governing equation for size-dependent vibration of electro-statically actuated nano-bridges made of functionally graded materials in the presence of surface effects and Casimir forces is developed. Based on Euler–Bernoulli beam theory, the displacement field can be expressed as follows:

$$u(x,z,t)=-z\theta(x,t)=-z\frac{\partial w}{\partial x}\qquad w=w(x,t) \tag{19}$$

The strain of a material point located at a distance z from the top plane for the nano-beam is represented as:

$$\varepsilon_{xx}=\frac{\partial u}{\partial x}=-z\frac{\partial^2w}{\partial x^2} \tag{20}$$

Based on the surface elasticity theory, the strain energy in the surface layer with zero thickness can be expressed as [43]:

$$U_s=\frac{1}{2}\int_0^l\int_S(\tau_{\alpha\beta}\varepsilon_{\alpha\beta}+\tau_{k\alpha}u_{k,\alpha})dSdx, \tag{21}$$

in which α, β denote the in-plane Cartesian coordination of the surface and k is the out-plane Cartesian coordination of the surface. Substituting equation (6) in equation (21) results in:

$$\begin{aligned}U_s&=\frac{1}{2}\int_0^l\int_S\left[\left(\tau_0+E_0\frac{\partial u}{\partial x}\right)\varepsilon_{xx}+\tau_0\left(\frac{\partial w}{\partial x}\right)^2\right]dSdx\\&=\frac{1}{2}\int_0^l\int_{S^+}\left[-\left(\tau_0^+-E_0^+z\frac{\partial^2w}{\partial x^2}\right)z\frac{\partial^2w}{\partial x^2}+\tau_0^+\left(\frac{\partial w}{\partial x}\right)^2\right]dS^+dx\\&\quad+\frac{1}{2}\int_0^l\int_{S^-}\left[-\left(\tau_0^--E_0^-z\frac{\partial^2w}{\partial x^2}\right)z\frac{\partial^2w}{\partial x^2}+\tau_0^-\left(\frac{\partial w}{\partial x}\right)^2\right]dS^-dx\end{aligned} \tag{22}$$

Simplifying the surface energy described in (22) yields:

$$U_s=\frac{1}{2}\int_0^l\left[\left(\tau_0^++\tau_0^-\right)S_0^*\left(\frac{\partial w}{\partial x}\right)^2+\left(E_0^++E_0^-\right)I_0^*\left(\frac{\partial^2w}{\partial x^2}\right)^2\right]dx \tag{23}$$

where for rectangular cross section $I_0^*=\int_{S^-}z^2dS^-=\int_{S^+}z^2dS^+=bh^2/4+h^3/12$ and $S_0^*=\int_{S^-}dS^-=\int_{S^+}dS^+=b$. Moreover, the virtual work W performed by the axial, electrical, Casimir and damping forces incorporating the von-Karman type nonlinear strain can be written as [44]:

$$W=-\frac{1}{2}\int_0^l\left(N_0+\frac{(EA)_{eq}}{2L}\int_0^l\left(\frac{\partial w}{\partial x}\right)^2dx\right)\left(\frac{\partial w}{\partial x}\right)^2dx+\int_0^l(F_e+F_C+F_d)wdx \tag{24}$$

where $F_d=-c\partial w/\partial t$ is the damping force $(EA)_{eq}$is the equivalent axial rigidity of FGM nano-beam which can be represented as:

$$(EA)_{eq}=\int_0^h\left[E^++\left(\frac{\tilde{z}}{h}\right)^n\left(E^--E^+\right)\right]bd\tilde{z}=\left(1+\frac{E_{mc}-1}{n+1}\right)bhE^+ \tag{25}$$

In which the non-dimensional parameters E_{mc} denotes the ratio of elastic modulus of the two FGM phases. The kinetic energies for the FG bulk material and surface layer are obtained as follows:

$$\begin{aligned}T&=\frac{1}{2}\int_0^l\int_A\rho(z)\left(\frac{\partial w}{\partial t}\right)^2dAdx+\frac{1}{2}\int_0^l\int_{S^+}\rho_0^+\left(\frac{\partial w}{\partial t}\right)^2dS^+dx\\&\quad+\frac{1}{2}\int_0^l\int_{S^-}\rho_0^-\left(\frac{\partial w}{\partial t}\right)^2dS^-dx=\frac{1}{2}\Big((\rho A)_{eq}\\&\quad+\left(\rho_0^++\rho_0^-\right)S_0^*\Big)\int_0^l\left(\frac{\partial w}{\partial t}\right)^2dx\end{aligned} \tag{26}$$

where

$$(\rho A)_{eq}=\int_0^h\left[\rho^++\left(\frac{\tilde{z}}{h}\right)^n\left(\rho^--\rho^+\right)\right]bd\tilde{z}=\left(1+\frac{\rho_{mc}-1}{n+1}\right)bh\rho^+ \tag{27}$$

in the aforementioned equation, ρ_{mc} is the ratio of density of the two FGM phases. The first variation of the strain energy is obtained as [45,46]:

$$\delta U_b=\int_0^l\int_A\sigma_{ij}\delta\varepsilon_{ij}dAdx \tag{28}$$

where A is the area of the cross-section of the nano-beam. Substituting Eq. (20) into Eq. (28), the variation of strain energy can be obtained as:

$$\delta U_b = -\int_0^l \int_A z\sigma_{xx}\frac{\partial^2 \delta w}{\partial x^2} dA dx = \int_0^l M(x,t)\left(\frac{\partial^2 \delta w}{\partial x^2}\right) dx \tag{29}$$

in which $M(x,t) = -\int_A \sigma_{xx} z dA$ is the local resultant bending moment of the nano-beam. Applying the Hamilton's principle results into:

$$\int_{t_1}^{t_2} (\delta T - [\delta U_b + \delta U_s] + \delta W) dt = 0 \tag{30}$$

After some mathematical computations, the nonlinear governing equation of motion is expressed as follows:

$$\begin{aligned}\frac{\partial^2 M}{\partial x^2} = &-\left((\rho A)_{eq} + \left(\rho_0^+ + \rho_0^-\right)S_0^*\right)\frac{\partial^2 w}{\partial t^2} - \left(E_0^+ + E_0^-\right)I_0^*\frac{\partial^4 w}{\partial x^4} \\ &+ \left(\tau_0^+ + \tau_0^-\right)S_0^*\frac{\partial^2 w}{\partial x^2} + \left(N_0 + \frac{(EA)_{eq}}{2L}\int_0^l \left(\frac{\partial w}{\partial x}\right)^2 dx\right)\frac{\partial^2 w}{\partial x^2} \\ &+ F_e + F_C - c\frac{\partial w}{\partial t}\end{aligned} \tag{31}$$

The corresponding boundary conditions at the ends of the nano-bridge require:

$$x = 0,\ l: \quad w = 0,\ \frac{\partial w}{\partial x} = 0 \tag{32}$$

Using the relation of the normal stress described in equations (3) and (6), the local resultant bending moment of the nano-beam is expressed as:

$$\begin{aligned}M(x,t) &= -\int_A \sigma_{xx} z dA \\ &= -\int_A \left(E(z)z\varepsilon_{xx} + \nu\left\{\frac{z}{2}\left[\left(\tau_0^+ - \tau_0^-\right)\left(\frac{\partial^2 w}{\partial x^2}\right) - \left(\rho_0^+ - \rho_0^-\right)\left(\frac{\partial^2 w}{\partial t^2}\right)\right]\right\} + \frac{z^2}{h}\left[\left(\tau_0^+ + \tau_0^-\right)\left(\frac{\partial^2 w}{\partial x^2}\right) - \left(\rho_0^+ + \rho_0^-\right)\left(\frac{\partial^2 w}{\partial t^2}\right)\right]\right\}\right) dA \\ &= (EI)_{eq}\frac{\partial^2 w}{\partial x^2} - \frac{\nu Ah}{4}\left(\left(\tau_0^+ - \tau_0^-\right)\frac{\partial^2 w}{\partial x^2} - \left(\rho_0^+ - \rho_0^-\right)\frac{\partial^2 w}{\partial t^2}\right) - \frac{\nu I}{h}\left(\left(\tau_0^+ + \tau_0^-\right)\frac{\partial^2 w}{\partial x^2} - \left(\rho_0^+ + \rho_0^-\right)\frac{\partial^2 w}{\partial t^2}\right)\end{aligned} \tag{33}$$

in which

$$(EI)_{eq} = \int_0^h z^2\left[E^+ + \left(\frac{\tilde{z}}{h}\right)^n\left(E^- - E^+\right)\right] b d\tilde{z} = \frac{bh^3}{12}E^+\tilde{\zeta}(n) \tag{34}$$

$$\tilde{\zeta}(n) = \frac{12E_{mc}^2 + (4n^3 + 16n^2 + 28n)E_{mc} + n^4 + 4n^3 + 7n^2}{(n + E_{mc})(n+3)(n+2)^2} \tag{35}$$

Assuming $\tau_{xx}^{nl} = \tau_{xx}$, $\tau_{zx}^{nl} = \tau_{zx}$ [27] and substituting equations (31) and (33) into equation (12), results in the explicit expression for the nonlocal bending moment M^{nl} as follows:

$$\begin{aligned}M^{nl} = &(EI)_{eq}\frac{\partial^2 w}{\partial x^2} - \frac{\nu Ah}{4}\left(\left(\tau_0^+ - \tau_0^-\right)\frac{\partial^2 w}{\partial x^2} - \left(\rho_0^+ - \rho_0^-\right)\frac{\partial^2 w}{\partial t^2}\right) \\ &- \frac{\nu I}{h}\left(\left(\tau_0^+ + \tau_0^-\right)\frac{\partial^2 w}{\partial x^2} - \left(\rho_0^+ + \rho_0^-\right)\frac{\partial^2 w}{\partial t^2}\right) \\ &+ (e_0 a)^2\left[-\left((\rho A)_{eq} + \left(\rho_0^+ + \rho_0^-\right)S_0^*\right)\frac{\partial^2 w}{\partial t^2}\right. \\ &\left. + \left(N_0 + \frac{(EA)_{eq}}{2L}\int_0^l \left(\frac{\partial w}{\partial x}\right)^2 dx\right)\frac{\partial^2 w}{\partial x^2} + F_e + F_C - c\frac{\partial w}{\partial t}\right]\end{aligned} \tag{36}$$

The governing equation of motion for the non-local nano-bridges can be obtained by inserting equation (36) into equation (31):

$$\begin{aligned}&(EI)_{eq}\frac{\partial^4 w}{\partial x^4} - \frac{\nu I}{h}\left(\left(\tau_0^+ + \tau_0^-\right)\frac{\partial^4 w}{\partial x^4} - \left(\rho_0^+ + \rho_0^-\right)\frac{\partial^4 w}{\partial x^2 \partial t^2}\right) - \frac{\nu Ah}{4}\left(\left(\tau_0^+ - \tau_0^-\right)\frac{\partial^4 w}{\partial x^4} - \left(\rho_0^+ - \rho_0^-\right)\frac{\partial^4 w}{\partial x^2 \partial t^2}\right) \\ &+ \left(E_0^+ + E_0^-\right)I_0^*\frac{\partial^4 w}{\partial x^4} - \left(\tau_0^+ + \tau_0^-\right)S_0^*\frac{\partial^2 w}{\partial x^2} = \left(1 - (e_0 a)^2\frac{\partial^2}{\partial x^2}\right)\left[-\left((\rho A)_{eq} + \left(\rho_0^+ + \rho_0^-\right)S_0^*\right)\frac{\partial^2 w}{\partial t^2}\right. \\ &\left. + \left(N_0 + \frac{(EA)_{eq}}{2L}\int_0^l \left(\frac{\partial w}{\partial x}\right)^2 dx\right)\frac{\partial^2 w}{\partial x^2} + F_e + F_C - c\frac{\partial w}{\partial t}\right]\end{aligned} \tag{37}$$

By assuming the same initial gaps from the bottom and top plates and introducing the following non-dimensional variables:

$$W=\frac{w}{g},\ \xi=\frac{x}{l},\ \overline{\tau}=\sqrt{\frac{E^{+}h^{2}}{12\rho^{+}l^{4}}}t,\ \varepsilon_0=\frac{e_0a}{l},\ C=cl\sqrt{\frac{12}{\rho^{+}b^{2}h^{4}E^{+}}},$$
$$\overline{V}_1^2=\frac{6\varepsilon_0\varepsilon l^4V_1^2}{E^{+}h^3g^3},\ \overline{V}_2^2=\frac{6\varepsilon_0\varepsilon l^4V_2^2}{E^{+}h^3g^3},\ f_\varepsilon=1+\frac{1}{\delta\varepsilon^{+}}\left(\frac{n}{n+1}\right),$$
$$\gamma=0.65\frac{g}{b},\ \lambda_C=\frac{\pi^2\hbar cl^4}{20E^{+}h^3g^5},\ f_\omega=\frac{c}{g\omega_p},\ f_0=\frac{12N_0l^2}{E^{+}bh^3},$$
$$\delta=\frac{g}{h},\ \sigma_1=\frac{12\left(E_0^{+}+E_0^{-}\right)I_0^{*}-bh^2\nu(\tau_0^{+}+\tau_0^{-})-3\nu bh^2(\tau_0^{+}-\tau_0^{-})}{E^{+}bh^3},$$
$$\sigma_2=\frac{12(\tau_0^{+}+\tau_0^{-})S_0^{*}l^2}{E^{+}bh^3},\ \kappa_1=\frac{\nu(\rho_0^{+}+\rho_0^{-})h+3(\rho_0^{+}-\rho_0^{-})}{12\rho^{+}l^2},$$
$$\kappa_2=\frac{(\rho_0^{+}+\rho_0^{-})S_0^{*}}{\rho^{+}bh},\tag{38}$$

the non-dimensional equation of motion for FGM nonlocal nano-beam vibration incorporating surface effects and dispersion forces can be written as:

$$\left(\tilde{\zeta}(n)+\sigma_1\right)\frac{\partial^4W}{\partial\xi^4}+\kappa_1\frac{\partial^4W}{\partial\xi^2\partial\overline{\tau}^2}-\sigma_2\frac{\partial^2W}{\partial\xi^2}=\left(1-\varepsilon_0^2\nabla^2\right)\left[\frac{\overline{V}_1^2}{(1-W)^2}+\frac{\gamma\overline{V}_1^2}{(1-W)}-\frac{\overline{V}_2^2}{(f_\varepsilon+W)^2}-\frac{\gamma\overline{V}_2^2}{(f_\varepsilon+W)}+\frac{\lambda_C}{(1-W)^4}-\frac{\lambda_C}{(1+W)^4}\right.$$
$$\left.+\frac{16\lambda_Cf_\omega}{3(1+W)^5}-\frac{24\lambda_Cf_\omega^2}{(1+W)^6}+\left(f_0+6\delta^2\tilde{E}(n)\int_0^1\left(\frac{\partial W}{\partial\xi}\right)^2d\xi\right)\frac{\partial^2W}{\partial\xi^2}-C\frac{\partial W}{\partial\overline{\tau}}-(\tilde{\rho}(n)+\kappa_2)\frac{\partial^2W}{\partial\overline{\tau}^2}\right]\tag{39}$$

with the following boundary conditions:

$$W(0,\overline{\tau})=W'(0,\overline{\tau})=W(1,\overline{\tau})=W'(1,\overline{\tau})=0\tag{40}$$

previous step [47]. If the time steps are selected small enough, accurate enough results is achieved. The reduced order models eliminate the spatial dependence in the PDEs using the Galerkin-based methods [48]. To this end, the displacements are expressed as a linear combination of independent basis functions. The basis set must satisfy the boundary conditions. By defining the orthogonality condition of the residue to every basis function, the second-order time-dependent ODEs in terms of the generalized co-ordinates (associated with the basis functions) can be obtained.

To obtain a Reduced-Order-Model (ROM), the non-dimensional deformation can be assumed as $W(\xi,\overline{\tau})=\sum_{j=1}^{N}T_j(\overline{\tau})\phi_j(\xi)$, where N denotes the number of considered modes and $\phi_j(\xi)$ is the jth mode shape of nano-bridge which can be written as:

$$\phi_j(\xi)=\cosh(\lambda_j\xi)-\cos(\lambda_j\xi)-\frac{\cosh(\lambda_j)-\cos(\lambda_j)}{\sinh(\lambda_j)-\sinh(\lambda_j)}(\sinh(\lambda_j\xi)-\sinh(\lambda_j\xi))\tag{41}$$

in which λ_j is the root of characteristic equation for jth eigenmode. By substituting equation (31) into equation (39), multiplying by $\phi_j(\xi)$ and integrating from $\xi=0$ to μ_{mc}, the Reduced-Order-Model based on the Bubnov–Galerkin decomposition procedure [48] can be expressed as:

$$\sum_{j=1}^{N}M_{ij}\ddot{T}_{ij}(\overline{\tau})+\sum_{j=1}^{N}K_{ij}T_{ij}(\overline{\tau})=F_i\tag{42}$$

in which

$$M_{ij}=(\tilde{\rho}(n)+\kappa_2)\int_0^1\varphi_i\varphi_jd\xi+[\kappa_1-\varepsilon_0(\tilde{\rho}(n)+\kappa_2)]\int_0^1\varphi_i\varphi_j''d\xi$$
$$K_{ij}=\left(\frac{3(n+1)\tilde{E}(n)-2n}{n+3}+\sigma_1\right)\int_0^1\varphi_i\varphi_j^{(iv)}d\xi-(f_0+\sigma_2)\int_0^1\varphi_i\varphi_j''d\xi+\varepsilon_0f_0\int_0^1\varphi_i\varphi_j^{(iv)}d\xi$$

3. Numerical analysis

In order to numerically study the dynamic behavior of FGM nano-bridge, the governing equation of motion (39) should be integrated over the time domain. For this purpose, in each time step of integration, the nonlinear terms on the right hand side of equation (39) are considered as a function of the values in the

where F_i describes the nonlinear terms. By integrating equation (42) over the time domain, the dynamic behavior of the system can be simulated.

$$F_i=\alpha\tilde{E}(n)\int_0^1\varphi_i\left(\sum_{j=1}^N\varphi_j''T_j\right)\left(\int_0^1\left(\sum_{j=1}^N\varphi_j'T_j\right)^2d\widehat{\xi}\right)d\xi-\varepsilon_0\alpha\tilde{E}(n)\int_0^1\varphi_i\left(\sum_{j=1}^N\varphi_j^{(iv)}T_j\right)\left(\int_0^1\left(\sum_{j=1}^N\varphi_j'T_j\right)^2d\widehat{\xi}\right)d\xi$$
$$+\int_0^1\varphi_i\left(\frac{\overline{V}_1^2\left(1+\gamma\left(f_\varepsilon-\sum_{j=1}^N\varphi_jT_j\right)\right)}{\left(1-\sum_{j=1}^N\varphi_jT_j\right)^2}-\frac{\overline{V}_2^2\left(1+\gamma\left(f_\varepsilon+\sum_{j=1}^N\varphi_jT_j\right)\right)}{\left(f_\varepsilon+\sum_{j=1}^N\varphi_jT_j\right)^2}\right)d\xi$$
$$-\varepsilon_0\int_0^1\varphi_i\left[\frac{6\overline{V}_1^2\left(1+\gamma\left(1-\sum_{j=1}^N\varphi_jT_j\right)\right)\left(\sum_{j=1}^N\varphi_j'T_j\right)^2}{\left(1-\sum_{j=1}^N\varphi_jT_j\right)^4}-\frac{4\overline{V}_1^2\gamma\left(\sum_{j=1}^N\varphi_j'T_j\right)^2}{\left(1-\sum_{j=1}^N\varphi_jT_j\right)^3}+\frac{2\overline{V}_1^2\left(1+\gamma\left(1-\sum_{j=1}^N\varphi_jT_j\right)\right)\left(\sum_{j=1}^N\varphi_j''T_j\right)}{\left(1-\sum_{j=1}^N\varphi_jT_j\right)^3}\right.$$
$$-\frac{\overline{V}_1^2\gamma\left(\sum_{j=1}^N\varphi_j''T_j\right)}{\left(1-\sum_{j=1}^N\varphi_jT_j\right)^2}-\frac{6\overline{V}_2^2\left(1+\gamma\left(f_\varepsilon+\sum_{j=1}^N\varphi_jT_j\right)\right)\left(\sum_{j=1}^N\varphi_j'T_j\right)^2}{\left(f_\varepsilon+\sum_{j=1}^N\varphi_jT_j\right)^4}+\frac{4\overline{V}_2^2\gamma\left(\sum_{j=1}^N\varphi_j'T_j\right)^2}{\left(f_\varepsilon+\sum_{j=1}^N\varphi_jT_j\right)^3}$$
$$\left.+\frac{2\overline{V}_2^2\left(1+\gamma\left(f_\varepsilon+\sum_{j=1}^N\varphi_jT_j\right)\right)\left(\sum_{j=1}^N\varphi_j''T_j\right)}{\left(f_\varepsilon+\sum_{j=1}^N\varphi_jT_j\right)^3}-\frac{\overline{V}_2^2\gamma\left(\sum_{j=1}^N\varphi_j''T_j\right)}{\left(f_\varepsilon+\sum_{j=1}^N\varphi_jT_j\right)^2}\right]d\xi+\lambda_C\int_0^1\varphi_i\left(\frac{1}{\left(1-\sum_{j=1}^N\varphi_jT_j\right)^4}-\frac{1}{\left(1+\sum_{j=1}^N\varphi_jT_j\right)^4}\right.$$
$$+\frac{16f_\omega}{3\left(1+\sum_{j=1}^N\varphi_jT_j\right)^5}-\frac{24f_\omega^2}{\left(1+\sum_{j=1}^N\varphi_jT_j\right)^6}\Bigg)d\xi-\varepsilon_0\lambda_C\int_0^1\varphi_i\left(\frac{4\left(\sum_{j=1}^N\varphi_j''T_j\right)}{\left(1-\sum_{j=1}^N\varphi_jT_j\right)^5}+\frac{20\left(\sum_{j=1}^N\varphi_j'T_j\right)^2}{\left(1-\sum_{j=1}^N\varphi_jT_j\right)^6}+\frac{160\left(\sum_{j=1}^N\varphi_j'T_j\right)^2}{\left(1-\sum_{j=1}^N\varphi_jT_j\right)^7}\right.$$
$$+\frac{1008\left(\sum_{j=1}^N\varphi_j'T_j\right)^2}{\left(1-\sum_{j=1}^N\varphi_jT_j\right)^8}+\frac{4\left(\sum_{j=1}^N\varphi_j''T_j\right)}{\left(1+\sum_{j=1}^N\varphi_jT_j\right)^5}-\frac{20\left(\sum_{j=1}^N\varphi_j'T_j\right)^2+80f_\omega/3\left(\sum_{j=1}^N\varphi_j''T_j\right)}{\left(1+\sum_{j=1}^N\varphi_jT_j\right)^6}$$
$$\left.-\frac{160\left(\sum_{j=1}^N\varphi_j'T_j\right)^2+144f_\omega^2\left(\sum_{j=1}^N\varphi_j''T_j\right)}{\left(1-\sum_{j=1}^N\varphi_jT_j\right)^7}+\frac{1008\left(\sum_{j=1}^N\varphi_j'T_j\right)^2}{\left(1-\sum_{j=1}^N\varphi_jT_j\right)^8}\right)d\xi \tag{43a}$$

4. Results and discussion

4.1. Validation of the present analysis

In order to validate the present numerical analysis, the values of dynamic pull-in voltage for the system, calculated by different methods, are presented in Table 1 using an example of 300 μm long, 20 μm wide and 2 μm thick double clamped beam with the initial gap $g_0 = 2$ μm. The beam is assumed to be made of single crystal silicon with Young modulus $E = 169$ GPa and Poisson's ratio $\nu = 0.28$ [49]. Since the width of the beam is much larger than its thickness, the Young modulus E is replaced by $\tilde{E} = E/(1-\nu^2)$. It is obvious that the values of computed dynamic pull-in voltage (V_{pid}) agrees well with those reported in the literature by using the reduced order model (ROM) with three modes and finite difference method [49]. Another comparison with experimental and theoretical results in the literature is performed using 100 μm wide and 1.5 μm thick micro-beams with initial gap of 1.18 μm. The effective Young's modulus for the micro-beams material is $\tilde{E} = 166$ GPa with a residual axial load $N_i = 0.0009$ N representative of pre-tensioned micro-beams [50]. Table 2 presents the calculated and empirical

Table 1
A comparison between dynamic pull-in voltages calculated by different methods.

Method	Present analysis	Three modes assumption	Reduced order model, three modes [49]	Finite difference [49]
V_{pid}	41.73	41.85	41.68	41.61

Table 2
Comparison between fundamental frequencies of micro-beams calculated by different methods.

Beam length (μm)	D.C. voltage (V)	$\omega/2\pi$ (kHz)				
		Present analysis	Measured [50]	Calculated [50]	Calculated [51]	HAM [52]
210	6.0	324.71	322.05	324.70	324.70	324.78
310	3.0	163.96	163.22	164.35	163.46	163.16
410	3.0	103.74	102.17	103.80	103.70	103.42

fundamental frequencies for vibrating pre-tensioned micro-bridges. This table reveals that the results of present model are in excellent agreement with the numerical and experimental results presented in the literature.

As another comparison, the dynamic pull-in voltage of a double-clamped silicon beam is considered. The geometrical properties of the beam is L = 1000 μm, b = 30 μm, b = 2.4 μm and g_0 = 10.1 μm. The material properties of the beam is ρ = 2231 kg/m^3, E = 97.5 GPa and υ = 0.26 GPa. The obtained results together with those reported in literature [53,54] are tabulated in Table 3. Krylov et al. [53] measured the pull-in voltage of the micro-beam (experimentally) as 100 V. On the other hand, Das and Batra [54] also determined the pull-in voltage of this beam based on the finite element analysis. They reported that the pull-in voltage of the microbeam is between 99 V and 100 V. As can be observed in Table 3, good agreement between the present method and those of literature is achieved.

To verify the results of the present analysis to predict the dynamic pull-in voltage for small-scale FGM beams, another comparison are conducted. The considered small-scale beam has the geometric and material properties as listed in Tables 4 and 5. The dynamic pull-in voltages of the micro-beam for different values of the power law exponent n are listed in Table 6. As can be seen, the obtained results are in a good agreement with those reported in Ref. [55]. On the other hand, one can observe that due to increasing in equivalent stiffness of the FGM micro-beam, the dynamic pull-in voltage is increased by increasing the value of gradient power n.

Table 3
A comparison between dynamic pull-in voltages of typical microbeam.

Method	Present modeling	Experiment [53]	Finite difference [54]
V_{pid}	98	100	99–100

Table 4
Material properties of FGM micro-beam.

Parameter	Length	Width	Thickness	Initial gap
Value	500 μm	100 μm	90 μm	2 μm

Table 5
Geometrical properties of FGM micro-beam.

Parameter	Value	
	Ceramic	Meta
Material type	Alumina (Al_2O_3)	Aluminum (Al)
Young's modulus (E)	390 GPa	70 GPa
Poisson's ratio (v)	0.22	0.228
Mass density (ρ)	3960 kg/m^3	2700 kg/m^3

Table 6
Dynamic pull-in voltage versus the gradient index n.

Gradient index n	$n = 5$	$n = 10$	$n = 20$	$n = 80$
Ref. [55]	93	100	104	108
Present analysis	93.78	100.41	104.03	108

4.2. Dynamic stability analysis

As the step DC voltage is applied on the nano-bridge, any increase in the actuation voltage leads to increase in the dynamic deflection until pull-in phenomenon occurs and the mid-point of nano-bridge adheres the substrate. This critical value of the applied voltage is known as dynamic pull-in voltage.

Fig. 3a–e represent the dynamic motion trajectories of the nano-bridge for different values of the actuation voltages V_1 and V_2, damping coefficient C and Casimir parameter λ_C, with different initial conditions. As indicated in Fig. 3a, when there is no applied voltage ($V_1 = V_2 = 0$) and for micro gaps ($\lambda_C = 0$), there exists only one stable center equilibrium position at zero ($W = 0$); for any initial condition, there is a limit cycle around the stable center point. However, it can be observed from Fig. 3b that in the presence of Casimir attraction ($\lambda_C \neq 0$), the first fixed point is a stable center and the second is an unstable saddle node. There exists a homoclinic orbit which starts from the unstable branch and goes back to the saddle node at the stable one. According to Fig. 3c, for double-side actuated nano-bridges and when there are no corrections in the governing equation, the phase portrait of the system has two saddle nodes and one stable center point. According to the properties of the stable node and the saddle point, there exist two heteroclinic orbits which depart from the unstable branch of one saddle point and arrive at the stable branch of the other one. The influence of damping parameter C on the dynamic behavior of vibrating nano-bridge is illustrated in Fig. 3d. The obtained results show that the stable center equilibrium point becomes a stable focus point when the damping parameter is taken into account. It can be concluded that the nano-bridge makes convergent oscillations near the focus point because of the damping, and shows periodic oscillations if the damping is neglected. As mentioned earlier, in this paper some modifications are considered in the governing equation. In order to demonstrate the effect of corrections on the dynamic behavior of the system, the phase portrait for $V_1 = V_2 = 7.5, f_\omega = 0.05$ is plotted in Fig. 3e. As seen, the heteroclinic orbits vanish and the homoclinic orbit appears in the phase portrait of the nano-structure. Fig. 3f illustrates the trajectory of the nano-bridge when the non-dimensional actuation parameters V_1 and V_2 increase to dynamic pull-in ones ($V_{pid} = 11.995$). In this state, the nano-structure becomes dynamically unstable for any initial conditions. There is no heteroclinic orbits and the physically center point coalesces with the saddle nodes.

4.3. Effect of nonlocal parameter

Tables 3 and 4 report the effect of nonlocal parameter (ε_0) on the dynamic pull-in voltage ($V_{pid,1}$) of the nano-bridge for various values of the gradient index and the Casimir parameter λ_C. The obtained results revealed that the nonlocal parameter induces a softening behavior i.e. the dynamic pull-in voltage of nano-bridge decreases with increasing the nonlocal parameter.

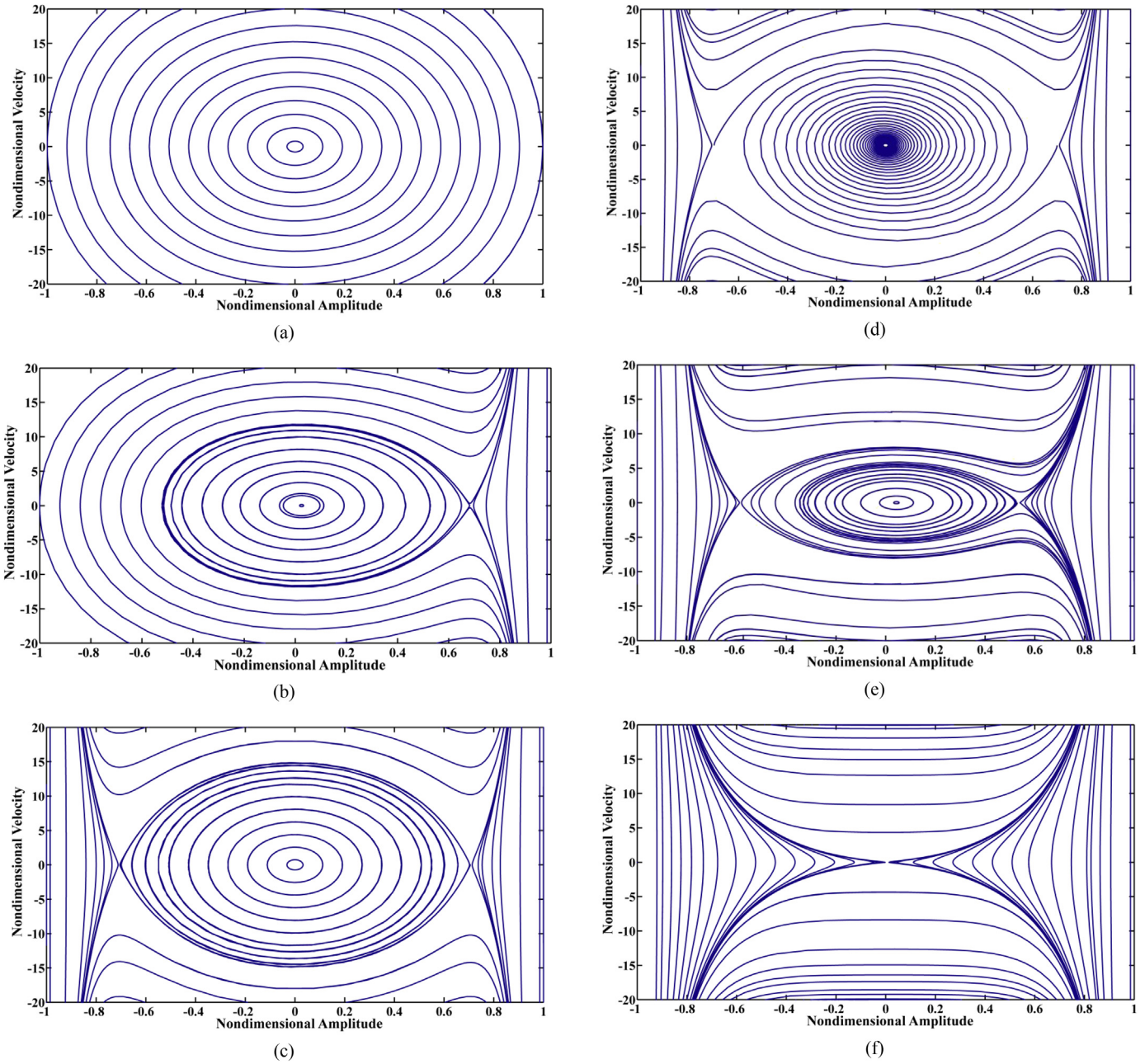

Fig. 3. Phase portraits of FGM nano-bridge for different initial conditions: (a) $\lambda_C = 0$, $V_1 = 0$, $V_2 = 0$ (b) $\lambda_C = 10$, $V_1 = 0$, $V_2 = 0$ (c) $\lambda_C = 10$, $V_1 = 0$, $V_2 = 0$ (d) $\lambda_C = 10$, $V_1 = 0$, $V_2 = 0$, $C = 2$ (e) $\lambda_C = 10$, $V_1 = 7.5$, $V_2 = 7.5$, $f_\omega = 0.05$ (f) $\lambda_C = 10$, $V_{pid,1} = 11.995$, $V_{pid,2} = 11.995$.

The values of the system parameters used in Table 7 are $\lambda_C = 10$, $f_0 = 1$, $E_{mc} = 1.5$, $\sigma_1 = -0.2$, $\sigma_2 = 5$, $V_2 = 0$, $\kappa_2 = 0.4$. It is observed from this table that the dynamic pull-in voltage decreases by increasing the nonlocal parameter ε_0. Moreover, the dynamic pull-in value decreases by increasing the gradient index n for $E_{mc} > 1$.

The impacts of nonlocal parameter on the instability behavior of the nano-bridges are tabulated in Table 8 for different values of

Table 7
Effects of gradient index n and nonlocal parameter on the dynamic pull-in voltage.

Nonlocal parameter (ε_0)	Dynamic pull-in voltage ($V_{pid,1}$)				
	$n = 1$	$n = 10$	$n = 20$	$n = 50$	$n = 100$
0	7.9658	7.4554	7.3309	7.2234	7.1772
0.1	7.8162	7.2995	7.1767	7.0697	7.0258
0.2	7.4432	6.9094	6.7904	6.6880	6.6464
0.3	6.9826	6.4236	6.3085	6.2113	6.1721
0.4	6.5301	5.9383	5.8261	5.7335	5.6964

Table 8
Effects of Casimir force and nonlocal parameter on the dynamic pull-in voltage.

Casimir parameter (λ_C)	Dynamic pull-in voltage ($V_{pid,1}$)				
	$\varepsilon_0 = 0$	$\varepsilon_0 = 0.1$	$\varepsilon_0 = 0.2$	$\varepsilon_0 = 0.3$	$\varepsilon_0 = 0.4$
0	9.1468	9.0669	8.8764	8.6621	8.4772
10	8.0749	7.9189	7.5278	7.0416	6.5608
20	7.1832	6.9567	6.3716	5.5849	4.7003
30	6.3605	6.0643	5.2685	4.1058	2.5241

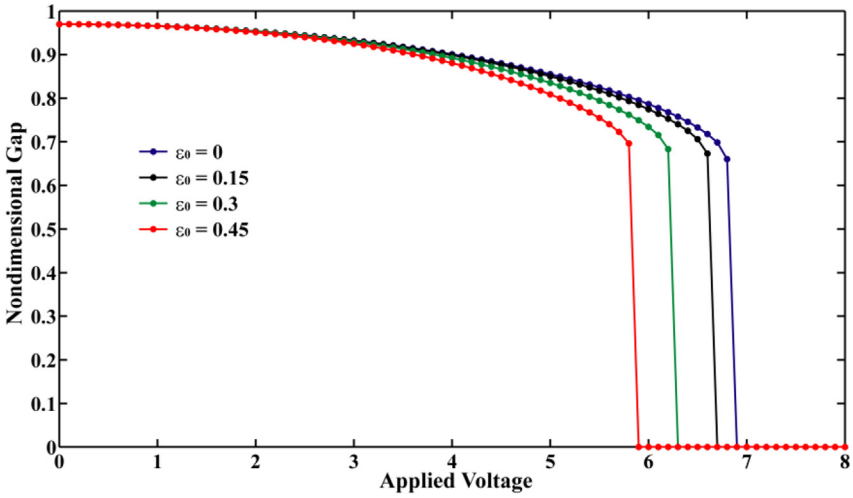

Fig. 4. Nondimensional gap versus the applied voltage of the lower plate for various values of nonlocal parameter and $n = 1$, $E_{mc} = 1.5$, $f_0 = 1$, $f_\omega = 0.05$, $\sigma_1 = 0.2$.

Casimir force. For micro-scale gap, the Coulomb force is dominant and dispersion forces might be neglected due to the large distance between the nano-bridge and the ground. However, if the distance between the moveable electrode and the ground is of the order of sub-micron, the presence of Casimir force should be taken into consideration. It appears from the obtained results that any increase in the Casimir force results in a significant decrease in the dynamic pull-in voltage. Moreover, Table 8 implies that effect of Casimir force is more pronounce for higher values of nonlocal parameters.

Fig. 4 reports the non-dimensional gap $(1-W)$ versus the voltage of the lower plate for different values of the nonlocal parameter ε_0. According to Fig. 4, it is clear that at the given value for DC voltage, the maximum deflection W of the system increases by increasing the nonlocal parameter. Furthermore, by increasing the nonlocal parameter, the mid-point of the nano-bridge deflects to the bottom substrate at lower values of applied voltage V_1. This means that the dynamic pull-in phenomenon occurs at lower values of actuation voltage V_1 as the size-effect parameter ε_0 increases.

4.4. Effect of surface layer

The influences of the surface stress and actuation voltage V_2 on the dynamic pull-in value of nonlocal FGM nano-bridge for $\varepsilon_0 = 0.1$ are listed in Table 9. One can observe that, any increase in the applied voltage of the upper electrode V_2 leads to a stabilizing effect i.e. increase in the dynamic pull-in voltage applied by the lower electrode. Furthermore, it is concluded from the reported results that the pull-in voltage decreases by decreasing the surface stress parameterσ_2.

Table 9
Effects of surface stress effect and the upper voltage V_2 on the dynamic pull-in voltage.

Applied voltage (V_2)	Dynamic pull-in voltage ($V_{pid,1}$)		
	$\sigma_2 = 5$	$\sigma_2 = 0$	$\sigma_2 = -5$
0	7.8162	7.7484	7.6798
2	7.9189	7.8519	7.7845
4	8.2253	8.1613	8.0968
6	8.7337	8.6746	8.6148

It can be seen from Eq. (39) that the non-dimensional parameter σ_1 which stands for the surface elastic modulus E_0 can affect the dynamic behavior of the nano-structure. Fig. 5 reports the non-dimensional gap versus the voltage of the lower plate for different values of the surface effect parameter σ_1. Fig. 5 shows the non-dimensional gap versus the applied voltage of the lower electrode under different values of σ_1. It can be seen that any increase in the σ_1 can decrease the pull-in voltage of the structure.

To investigate the influence of surface layer on the pull-in time of nano-bridge, the time history of FGM nano-beam at the corresponding dynamic pull-in voltages for several values of non-dimensional parameter σ_1 is illustrated in Fig. 6. According to the reported results, it is concluded that by increasing the surface effect parameter σ_1, the pull-in time decreases. Moreover, by increasing the parameter σ_1, the pull-in happens at larger values of mid-point deflection of the nano-bridge.

4.5. Effect of finite conductivity

Previous experimental measurements by the rotational NEMS devices imply the importance of the finite conductivity correction in simulating the NEMS fabricated from finite-conductive and non-metallic materials [42,56]. It is reported that without considering the finite conductivity, the experimental data are in disagreement with the ideal metal Casimir force whereas the inclusion of the finite conductivity correction leads to excellent agreement between the data and theory [42,56]. Indeed, the finite conductivity of the constitutive material reduces the Casimir force.

To investigate the influence of modifications due to finite conductivity of FG materials on the instability of the FGM nano-bridge, the dynamic pull-in voltage as a function of small-size parameter (ε_0) is plotted in Fig. 7. One can observe that the dynamic pull-in value decreases by increasing the non-local parameter until the critical point which the flexible electrode collapses onto the rigid electrode without any applied actuation. According to the illustrated results, it is concluded that if the Coulomb force correction is taken into account, the pull-in voltage shifts upward. The differences between the predicted values of pull-in voltages are very significant at lower values of nonlocal parameter. Similarly, incorporating the Casimir force correction results in lower values of pull-in voltage due to the lower strength of Casimir attraction. It is also inferred that for high values of nonlocal parameter, the effect of

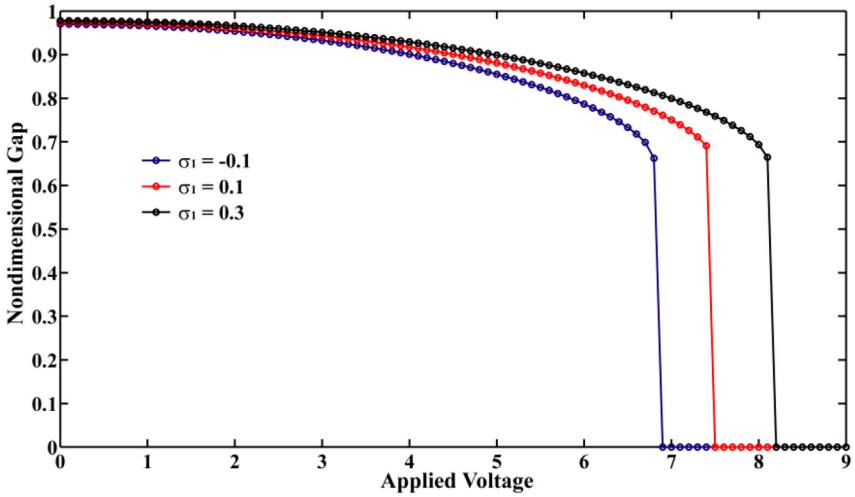

Fig. 5. Nondimensional gap versus the applied voltage of the lower plate for various values of surface elasticity parameter and $\varepsilon_0 = 0$, $n = 1$, $E_{mc} = 1.5$, $f_0 = 1$, $\kappa_2 = 0.4$, $\sigma_2 = 5$.

Casimir force correction on the instability is more significant in comparison with the Coulomb force correction.

For better understanding the importance of finite conductivity, the dynamic stability of freestanding nanobridge is investigated. A NEMS device might adhere to its substrate due to Casimir force (even without an applied voltage), if the minimum gap between the electrode and substrate is not considered. Besides interfering with the stability of freestanding nanostructures, the Casimir force can also induce undesired adhesion during the fabrication stages. The maximum permissible length of the nanowire L_{max}, which is required to prevent stiction, is called the detachment length [57,58]. For a given gap value, if the length of the nanowire exceeds L_{max}, then the movable electrode sticks to the ground. Thus, the maximum length is very important in design and fabrication of the nanostructure. By substituting the critical value of λ_c into the definition of λ_c (Eq. (38)), the L_{max} can be determined. As a case study, Fig. 8a shows the variation of L_{max} as a function of initial gap and thickness for typical gold (Au) beam. As seen, this finding reveals that Casimir force can substantially affect the stability of freestanding nano-bridge in sub-micron scales. One can observe that if the finite conductivity is taken into consideration, the detachment length increases because of the reduction of Casimir force. It should be noted that if the nano-beam length is greater than the detachment length, any undesirable disturbance in the fabrication process results in the instability of the structure even in the absence of any actuation voltages. The influence of non-local parameter on the instability of freestanding double-side nano-bridges is also investigated in Fig. 8b by plotting the variation of L_{max} as a function beam thickness. According to the illustrated results, it is concluded that L_{max} decreases by increasing the non-local parameter and the thickness of the nano-bridge will increase the detachment length of the system.

4.6. Effect of material composition

Fig. 9 illustrates the dimensionless gap versus the voltage of the lower plate for different values of gradient index n. From Fig. 9, one can observe that when the gradient index n increases, the dynamic pull-in voltage decreases and pull-in instability happens at lower values of applied voltage V_1.

Fig. 10 shows the impact of material properties on the dynamic pull-in voltage of the considered nonlocal nano-bridge using different values of non-dimensional parameter E_{mc} by varying the gradient index n. It appears from the illustrated results that for $E_{mc} > 1$, the dynamic pull-in voltage decreases by increasing the gradient power index. On the other hand, if $E_{mc} < 1$, the instability voltage decreases by increase in gradient index. This figure also shows that if the power n approaches to infinity, the values of pull-in voltages tend toward to the pull-in voltage of isotropic material with $E_{mc} = 1$.

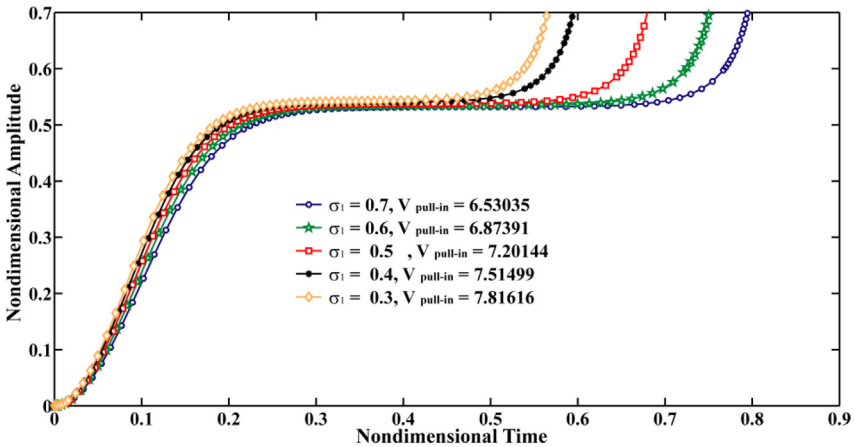

Fig. 6. History of vibrating FGM nano-bridge for different values of σ_1 at corresponding dynamic pull-in voltage for $\lambda_C = 10$, $\varepsilon_0 = 0.1$, $n = 1$, $E_{mc} = 0.1$, $f_0 = 1$, $\kappa_2 = 0.4$, $\sigma_2 = 5$, $V_2 = 0$.

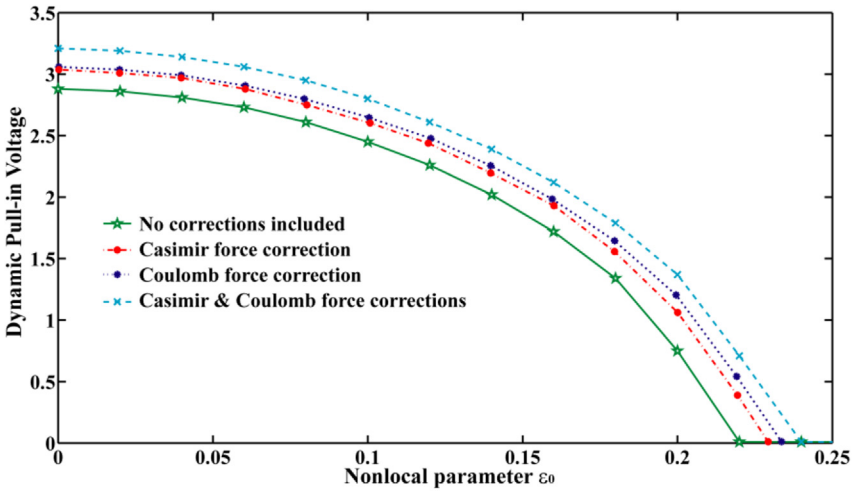

Fig. 7. Effect of finite conductivity correction on the dynamic pull-in voltage vs. nonlocal parameter.

4.7. Bifurcation analysis

In this section, the stability analysis of the nano-beam is investigated. To this end, the governing integro-partial differential equation (39) for FGM actuated nano-bridge has been reduced to a single-degree of freedom (SDOF) model using Bubnov–Galerkin based reduced order model (ROM). Thereby, the response of the non-linear system is assumed to be in the form:

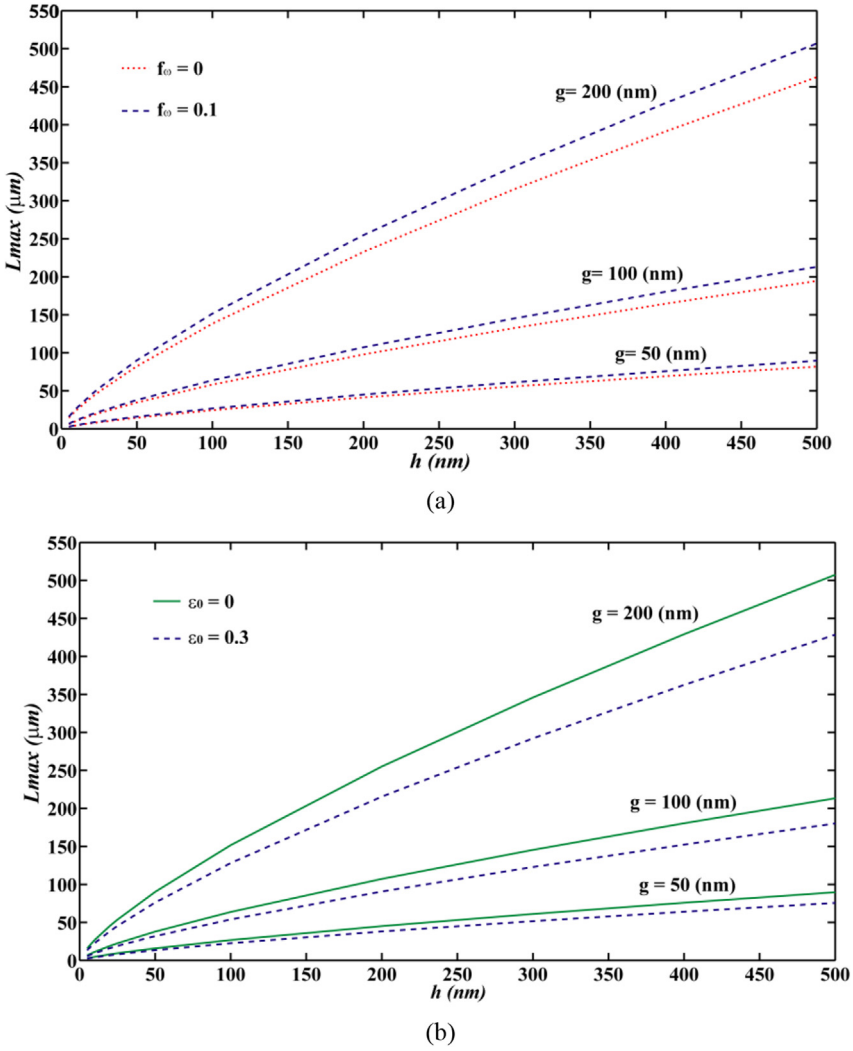

Fig. 8. Variation of the detachment length, L_{max} of freestanding double-side nano-bridge for various initial gap and thickness (a) effect of finite conductivity (b) effect of nonlocal parameter.

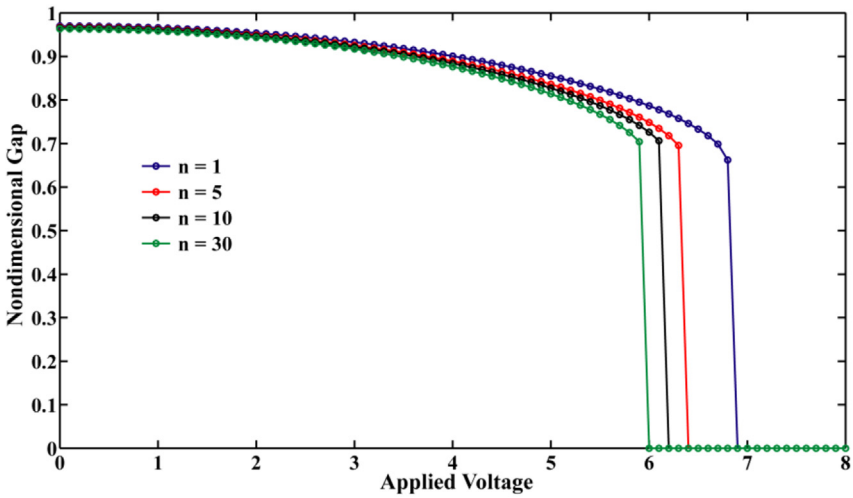

Fig. 9. Nondimensional gap versus the applied voltage of the lower plate for various values of gradient power and $\varepsilon_0 = 0$, $E_{mc} = 1.5$, $f_\omega = 0.05$.

$$W(\xi,\overline{\tau}) = q_1(\overline{\tau})\phi_1(\xi) \tag{43b}$$

where $\phi_1(\xi)$ is the first mode shape of double-clamped nano-beam and $q_1(\overline{\tau})$ is the time-dependent function that serves as the generalized temporal coordinate of SDOF model. After some computations, the governing equation (39) is reduced to:

$$M\ddot{T}(\overline{\tau}) + KT(\overline{\tau}) = F(T(\overline{\tau})) \tag{44}$$

By setting $T(\overline{\tau}) = q_1$, $dT(\overline{\tau})/d\overline{\tau} = q_2$, the ordinary differential equation (44) can be transformed into the following state-space form:

$$\begin{aligned} \frac{dq_1}{d\overline{\tau}} &= q_2 \\ \frac{dq_2}{d\overline{\tau}} &= -\frac{K}{M}q_1 - F(q_1,q_2) \end{aligned} \tag{45}$$

Thereby, the equilibrium points of the system can be obtained by setting the left-hand sides of equation (45) equal to zero. In order to construct the bifurcation diagram, the positions of the equilibrium points versus the actuation voltage as a control parameter must be plotted. On the other hand, in order to investigate the stability of the fixed-points, the following Jacobian matrix is used:

$$J = \begin{bmatrix} 0 & 1 \\ -\dfrac{K}{M} - \dfrac{\partial F(q_1,q_2)}{\partial q_1} & 0 \end{bmatrix} \tag{46}$$

if λ denotes the eigenvalue of the Jacobian matrix, for $\lambda^2 < 0$, the system has two pure imaginary roots, which means that the equilibrium point is a stable center point; whereas, for $\lambda^2 > 0$, the eigenvalues are real and have opposite signs, hence the fixed point is an unstable saddle node. In Fig. 11, solid and dashed curves represent the stable and unstable fixed points, respectively. As illustrated in Fig. 11, for $V < V_{pid}$ there exist two fixed points. The first equilibrium point is stable center and the other one is an unstable saddle node. Moreover, it is inferred that by increasing the actuation voltage, the distance between two fixed points decreases and for a critical voltage namely the "pull-in value", they coalesce in a saddle node bifurcation.

To examine the effect of double-side actuation on the dynamics of the considered nano-structure, the bifurcation diagram for the

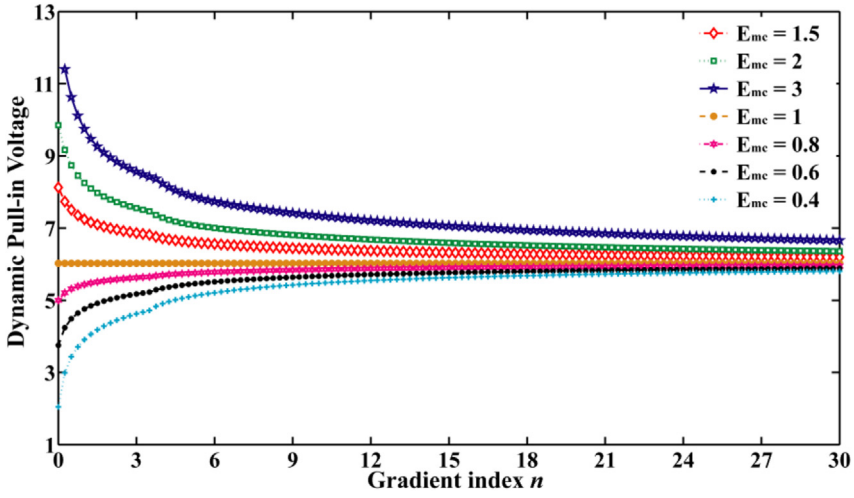

Fig. 10. Dynamic pull-in voltage vs. gradient index n and the parameter E_{mc} in the absence of surface effect for $\lambda_C = 10$, $f_0 = 1$, $\gamma = 0.195$, $\varepsilon_0 = 0.1$, $V_2 = 0$.

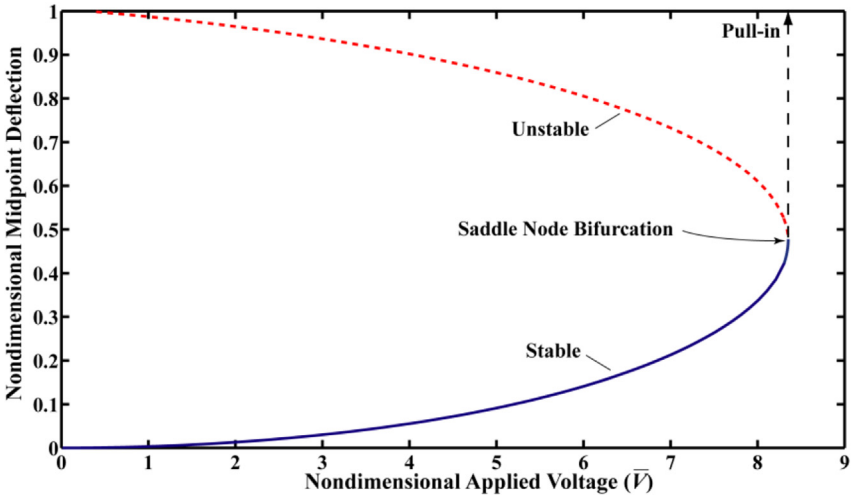

Fig. 11. Bifurcation diagram for nano-bridge under one-side actuation.

identical applied voltages ($V_1 = V_2 = V$) is shown in Fig. 12. One can observe that the pull-in instability is the subcritical pitchfork bifurcation, two unstable equilibria exist along with the stable center point for $V < V_{pid}$ and no stable equilibrium exists for the voltages higher than the pull-in value. In other words, the origin is stable for $V < V_{pid}$ and unstable for $V > V_{pid}$.

Finally, the influence of the Casimir parameter λ_C on the dynamic stability of double-sided actuated nano-beams is studied in Fig. 13. It is concluded that by increasing the Casimir parameter, the distance between the unstable saddle nodes decreases and the bifurcation point happens at lower values of applied voltage.

5. Concluding remarks

Herein, the nonlocal elasticity was employed to study the dynamic stability of double-sided asymmetric NEMS FGM bridges incorporating the effects of surface energy and finite conductivity of FGM. It was observed that:

1- The pull-in voltage increases by increasing the surface stress parameter. On the other hand, increasing the elastic modulus of surface layer, can increase or decrease the pull-in voltage depending on the sign of the elastic modulus of the surface layer.
2- The impact of finite conductivity of FG materials on the instability of nano-bridges was investigated by considering corrected Coulomb and Casimir force corrections. It is found that neglecting the finite conductivity of FGM leads to underestimate the computed pull-in voltage and maximum length of the freestanding nano-bridge.
3- The obtained results revealed that the nonlocal parameter induces a softening behavior i.e. the dynamic pull-in voltage of nano-bridge decreases with increasing the nonlocal parameter. Moreover, effect of Casimir force becomes more pronounce by increasing the nonlocal parameter value.
4- Freestanding micro-bridge (no Coulomb and Casimir forces) exhibits periodic motion around the stable center point. For single-side actuated nano-bridge under Casimir attraction, an unstable saddle node appears in the phase plane and there exists a homoclinic orbit which starts from the unstable branch and turns back to it at the stable one. For double-sided actuated nano-bridge, when the considered model was modified, the heteroclinic orbits vanished and the homoclinic orbit appeared in the phase portrait of the nano-

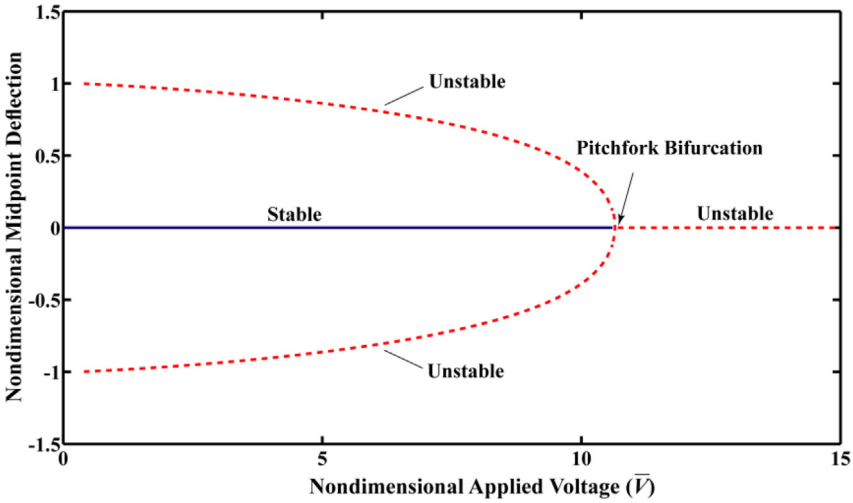

Fig. 12. Bifurcation diagram for nano-bridge under double-side actuation.

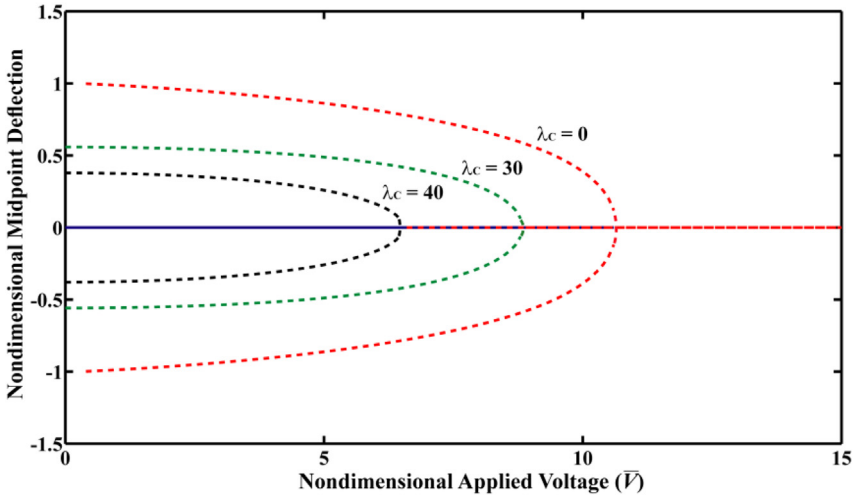

Fig. 13. Bifurcation diagram of nano-bridge under double-side actuation for different values of Casimir parameter λ_C.

structure. When the actuation voltage exceeds dynamic pull-in value, there is no heteroclinic orbits and the physically center point coalesces with the saddle points.

References

[1] Hasanyan DJ, Batra RC, Harutyunyan S. Pull-in instabilities in functionally graded microthermoelectromechanical systems. J Therm Stresses 2008;31(10):1006–21.
[2] Lü CF, Chen WQ, Lim CW. Elastic mechanical behavior of nano-scaled FGM films incorporating surface energies. Compos Sci Technol 2009;69:1124–30.
[3] Eltaher MA, Emam SA, Mahmoud FF. Static and stability analysis of nonlocal functionally graded nanobeams. Compos Struct 2013;96:82–8.
[4] Ke LL, Wang YS. Size effect on dynamic stability of functionally graded microbeams based on a modified couple stress theory. Compos Struct 2011;93:342–50.
[5] Arbind A, Reddy JN. Nonlinear analysis of functionally graded microstructure-dependent beams. Compos Struct 2013;98:272–81.
[6] Zeighampour H, Tadi Beni Y. Free vibration analysis of axially functionally graded nanobeam with radius varies along the length based on strain gradient theory. Appl Math Model 2015;39(18):5354–69.
[7] Fu YQ, Du HJ, Huang WM, Zhang S, Hu M. TiNi-based thin films in MEMS applications: a review. Sensors Actuat A 2004;112(2–3):395–408.
[8] Witvrouw A, Mehta A. The use of functionally graded poly-SiGe layers for MEMS applications. Funct Graded Mater 2005;8:255–60.
[9] Lee Z, Ophus C, Fischer LM, et al. Metallic NEMS components fabricated from nanocomposite Al-Mo films. Nanotechnology 2006;17(12):3063–70.
[10] Abbasnejad B, Rezazadeh G, Shabani R. Stability analysis of a capacitive fgm micro-beam using modified couple stress theory. Acta Mech Solid Sin 2013;26(4):427–40.
[11] Ji XL, Yang J, Kitipornchai S, Lim CW. Pull-in instability and free vibration of electrically actuated poly-SiGe graded micro-beams with a curved ground electrode. Appl Math Model 2012;36(5):1875–84.
[12] Sedighi HM, Daneshmand F, Abadyan MR. Dynamic instability analysis of electrostatic functionally graded doubly-clamped nano-actuators. Compos Struct 2015;124:55–64.
[13] Batra RC, Porfiri M, Spinello D. Effects of Casimir force on pull-in instability in micromembranes. EPL (Euro Phys Lett) 2007;77(2). http://dx.doi.org/10.1209/0295-5075/77/20010.
[14] Lamoreaux SK. The Casimir force: background, experiments, and applications. Rep Prog Phys 2005;68:201–36.
[15] Noruzifar E, Emig T, Zandi R. Universality versus material dependence of fluctuation forces between metallic wires. Phys Rev A 2011;84:042501.
[16] Hargreaves CM. Corrections to the related dispersion force between metal bodies. In: Proc. Kon. Ned. Akad. Wetenshap; 1965. p. 68231. Ser. B.
[17] Bezerra VB, Klimchitskaya GL, Romero C. Casimir force between a flat plate and a spherical lens: application to the results of a new experiment. Mod Phys Lett A 1997;12(34):2613–22.
[18] Wang ZQ, Zhao YP, Huang ZP. The effects of surface tension on the elastic properties of nano structures. Int J Eng Sci 2010;48:140–50.
[19] Gurtin ME, Murdoch AI. Surface stress in solids. Int J Solids Struct 1978;14:431–40.
[20] Shaat M, Mahmoud FF, Alieldin SS, Alshorbagy AE. Finite element analysis of functionally graded nano-scale films. Finite Elem Analysis Des 2013;74:41–52.
[21] Wang J, Huang Z, Duan H, Yu S, Feng X, Wang G, et al. Surface stress effect in mechanics of nanostructured materials. Acta Mech Solid Sin 2011;24(1):52–82.
[22] Sedighi HM. The influence of small scale on the pull-in behavior of nonlocal nanobridges considering surface effect, Casimir and van der waals attractions. Int J Appl Mech 2014;6(3):22. http://dx.doi.org/10.1142/S1758825114500306.
[23] Koochi A, Kazemi A, Khandani F, Abadyan M. Influence of surface effects on size-dependent instability of nano-actuators in the presence of quantum vacuum fluctuations. Phys Scr 2012;85(3):035804. http://dx.doi.org/10.1088/0031-8949/85/03/035804.
[24] Ansari R, Gholami R, Faghih Shojaei M, Mohammadi V, Sahmani S. Surface stress effect on the pull-in instability of circular nanoplates. Acta Astronaut 2014;102:140–50.
[25] Hosseini-Hashemi S, Nazemnezhad R. An analytical study on the nonlinear free vibration of functionally graded nanobeams incorporating surface effects. Compos Part B Eng 2013;52:199–206.
[26] Eringen AC. Linear theory of nonlocal elasticity and dispersion of plane waves. Int J Eng Sci 1972;10:425–35.
[27] Li C, Lim CW, Yu JL, Zeng QC. Analytical solutions for vibration of simply supported nonlocal nanobeams with an axial force. Int J Struct Stab Dyn 2011;11(2):257–71.
[28] Jun Yu Y, Tian XG, Liu XR. Size-dependent generalized thermoelasticity using Eringen's nonlocal model. Eur J Mech A Solids 2015;51:96–106.
[29] Reddy JN, El-Borgi S. Eringen's nonlocal theories of beams accounting for moderate rotations. Int J Eng Sci 2014;82:159–77.
[30] Kiani K. Nonlocal and shear effects on column buckling of single-layered membranes from stocky single-walled carbon nanotubes. Compos Part B Eng 2015;79:535–52.
[31] Jung WY, Han SC, Park WT. A modified couple stress theory for buckling analysis of S-FGM nanoplates embedded in pasternak elastic medium. Compos Part B Eng 2014;60:746–56.
[32] Ebrahimi F, Salari E. Size-dependent free flexural vibrational behavior of functionally graded nanobeams using semi-analytical differential transform method. Compos Part B Eng 2015;79:156–69.
[33] Ebrahimi F, Salari E. Thermo-mechanical vibration analysis of nonlocal temperature-dependent FG nanobeams with various boundary conditions. Compos Part B Eng 2015;78:272–90.
[34] Reddy JN, Praveen GN. Nonlinear transient thermoelastic analysis of functionally graded ceramic-metal plate. Int J Solids Struct 1998;35:4457–76.
[35] Lu P, He LH, Lee HP, Lu C. Thin plate theory including surface effects. Int J Solids Struct 2006;44:4631–47.
[36] Fu Y, Zhang J. Size-dependent pull-in phenomena in electrically actuated nanobeams incorporating surface energies. Appl Math Model 2011;35:941–51.
[37] Simsek M, Yurtcu HH. Analytical solutions for bending and buckling of functionally graded nanobeams based on the nonlocal Timoshenko beam theory. Compos Struct 2013;97:378–86.
[38] Mahmoud FF, Eltaher MA, Alshorbagy AE, Meletis EI. Static analysis of nanobeams including surface effects by nonlocal finite element. J Mech Sci Technol 2012;26(11):3555–63.
[39] Rong H, Huang QA, Nie M, Li W. An analytical model for pull-in voltage of clamped–clamped multilayer beams. Sensors Actuat A 2004;116:15–21.
[40] Lambrecht A, Jaekel MT, Reynaud S. The Casimir force for passive mirrors. Phys Lett A 1997;225:188–94.
[41] Mostepanenko VM, Trunov NN. The Casimir effect and its applications. Oxford: Oxford Science Publications; 1997.

[42] Lamoreaux SK. Calculation of the Casimir force between imperfectly conducting plates. Phys Rev A 1999;59(5):3149–53.
[43] Shaat M, Mohamed SA. Nonlinear-electrostatic analysis of micro-actuated beams based on couple stress and surface elasticity theories. Int J Mech Sci 2014;84:208–17.
[44] Batra RC, Porfiri M, Spinello D. Vibrations of narrow microbeams predeformed by an electric field. J Sound Vib 2008;309:600–12.
[45] Soltani P, Kassaei A, Taherian MM. Nonlinear and quasi-linear behavior of a curved carbon nanotube vibrating in an electric force field; an analytical approach. Acta Mech Solid Sin 2014;27(1):97–110.
[46] Rahmani O, Pedram O. Analysis and modeling the size effect on vibration of functionally graded nanobeams based on nonlocal Timoshenko beam theory. Int J Eng Sci 2014;77:55–70.
[47] Valilou S, Rezazadeh G, Shabani R, Fathalilou M. Bifurcation analysis of a capacitive micro-resonator considering non-local elasticity theory. Int J Nonlinear Sci Numer Simul 2014;15(5):241–9.
[48] Nayfeh AH, Younis MI, Abdel-Rahman EM. Reduced-order models for MEMS applications. Nonlinear Dyn 2005;41(1–3):211–36.
[49] Krylov S. Lyapunov exponents as a criterion for the dynamic pull-in instability of electrostatically actuated microstructures. Int J Non-linear Mech 2007;42:626–42.
[50] Tilmans HA, Legtenberg R. Electrostatically driven vacuum-encapsulated polysilicon resonators. Part II: theory and performance. Sens Actuat A 1994;45(1):67–84.
[51] Kuang JH, Chen CJ. Dynamic characteristics of shaped micro-actuators solved using the differential quadrature method. J Micromech Microeng 2004;14(4):647–55.
[52] Moghimi Zand M, Ahmadian MT. Application of homotopy analysis method in studying dynamic pull-in instability of microsystems. Mech Res Commun 2009;36:851–8.
[53] Krylov S, Ilic BR, Schreiber D, Seretensky S, Craighead H. The pull-in behavior of electrostatically actuated bistable microstructures. J Micromech Microeng 2008;18(055026):20.
[54] Das K, Batra RC. Pull-in and snap-through instabilities in transient deformations of microelectromechanical systems. J Micromech Microeng 2009;19(035008):19.
[55] Abbasnejad B, Rezazadeh G. Mechanical behavior of a FGM micro-beam subjected to a nonlinear electrostatic pressure. Int J Mech Mater Des 2012;8:381–92.
[56] Klimchitskaya GL, Mohideen U, Mostepanenko VM. The Casimir force between real materials: experiment and theory. Rev Mod Phys 2009;81.
[57] Lin WH, Zhao YP. Nonlinear behavior for nanoscale electrostatic actuators with Casimir force, Chaos. Solit Fractals 2005;23:1777–85.
[58] Lin WH, Zhao YP. Casimir effect on the pull-in parameters of nanometer switches. Microsyst Technol 2005;11:80–5.